General Disclaimer

One or more of the Following Statements may affect this Document

- This document has been reproduced from the best copy furnished by the organizational source. It is being released in the interest of making available as much information as possible.

- This document may contain data, which exceeds the sheet parameters. It was furnished in this condition by the organizational source and is the best copy available.

- This document may contain tone-on-tone or color graphs, charts and/or pictures, which have been reproduced in black and white.

- This document is paginated as submitted by the original source.

- Portions of this document are not fully legible due to the historical nature of some of the material. However, it is the best reproduction available from the original submission.

Produced by the NASA Center for Aerospace Information (CASI)

ON THE DETERMINATION
OF ATMOSPHERIC PATH LENGTH
BY PASSIVE MICROWAVE RADIOMETER

WILLIAM J. WEBSTER, JR.

MAY 1975

GODDARD SPACE FLIGHT CENTER —
GREENBELT, MARYLAND

ON THE DETERMINATION
OF ATMOSPHERIC PATH LENGTH
BY PASSIVE MICROWAVE RADIOMETER

William J. Webster, Jr.

ABSTRACT

The Pacific Plate Motion Experiment (PPME) will use int.   ometry tech-
niques to make precise measurements of geophysical   . At the level of
accuracy required, the path length error due to the neut   lov er atmosphere
makes a significant contribution to the error budget of the interferometer
measurements. In order to better define the needs of the PPME, this review
and study was prepared.

A review of previous work shows that, while very little has been published on
the small-scale distribution of the atmospheric water vapor, the large-scale
distribution of water vapor is known to vary significantly over time scales as
short as 20 minutes. This variation in water vapor content is the main source
of the changes in path length error at a particular site.

It is shown that the current "state of the art" in passive microwave radiometry
allows a very precise measurement of the brightness temperature of the sky.
It is also noted that the technological requirements of radiometers are very
different from the requirements of radio astronomy. The technology has been
used in the construction of radiometers which are sufficient for use in the path
length correction problem.

A simulation study shows that, when combined with surface meteorology data,
passive microwave radiometer data will allow a determination of the path
length correction to better than 2 cm at the zenith. By a careful choice of
frequencies, a dual frequency system will allow a measurement of the path
length correction to better than 4 cm at zenith angles as great as 60°. Be-
cause of the wide range of weather conditions to be expected for the PPME
sites (which include Alaska, Hawaii and Massachusetts), it will probably be
necessary to use a separate correction algorithm for each site.

CONTENTS

ILLUSTRATIONS

TABLES

I. THE PATH LENGTH PROBLEM

The atmospheric path length differs from the geometric path length because of the influence of the index of refraction of the atmosphere. If $\bar{r}$ is the vector from the observer to the object of interest, the difference between the geometric and apparent path length $(\bar{R})$ is given by:

$$\bar{R} = \int_a^b (n - 1)\, d\bar{r} \tag{1}$$

where the observer is at point a, the object is at point b and n is the index of refraction.

Any precise measurement of a length within the atmosphere requires a correction for the path length error due to the atmosphere. Obviously, the importance of the correction increases as the geometric path length increases until the entire atmosphere is included. For example, the path length correction for the zenith direction through the entire atmosphere is about 2.2 meters for frequencies around 3 GHz.

In this paper, we will deal with the problem of path length corrections in the 1.4 GHz to 10 GHz frequency range. As contrasted with the optical problem or the millimeter wavelength problem, the following conditions hold:

1. Dispersive (i.e., frequency dependent) effects are negligible. Calculations show that at most 10^{-6} of the path length correction at 10 GHz is due to dispersive effects.

2. Clouds are nearly transparent. Except for the highest frequencies, even heavy rain clouds are not opaque.

3. The dominant influence on the variation of the path length is the distribution of atmospheric water vapor and its changes. As we will see, the index of refraction of the dry atmosphere is relatively constant, while the index of refraction due to water vapor is highly variable. In a sense, the dry atmosphere sets the average path length error while the water vapor is responsible for the variations.

Bean and Dutton (1966) have shown that the radio refractive index can be approximated by:

$$n - 1 = \frac{A}{T}\left\{P + \frac{Be}{T}\right\} \tag{2}$$

where e is the partial pressure of water vapor (mb), T is the temperature ($^{\circ}$K) and P is the atmospheric pressure (mb). A and B are constants (A = 77.6 x $10^{-6} \frac{^{\circ}K}{mb}$, B = 4810 $^{\circ}$K). Substituting into (1) and using the ideal gas law yields, for the zenith direction:

$$R(cm) = 0.277\ P(o) + \int_0^\infty \frac{Ce(h)}{T^2(h)}\ dh \tag{3}$$

where h is the altitude above the surface (cm) and C is a constant.

Clearly, at a minimum, the surface pressure and the altitude distributions of water vapor and temperature are required to determine R.

Of the approximately 2.2 m of typical path length, equation (3) shows that about 1.5 meter is due to the dry atmosphere. Since seasonal variations of the partial pressure of water vapor can be as much as 100% there can be variations of nearly half a meter in the water vapor contribution to the correction.

Numerous studies have obtained approximations to the path length correction based on atmospheric statistics and surface meteorological measurements (i.e., Hopfield, 1971; Marini and Murray, 1973). The conclusions have usually been that the correction schemes are accurate to about 2 cm for the zenith. However, a recent study (Goad, 1974) shows that, when the various formulations are used for a site which was not included in the original statistical ensemble, the predictions are accurate to 5 cm at best for the zenith and become progressively poorer as the zenith angle increases. Since the contribution of the atmospheric path length error to the accuracy of the PPME baseline measurements can be considerable, it is necessary to measure the path length correction to 2 cm or better accuracy at the zenith.

Because of the difficulty of implementing active sounding techniques near a high sensitivity receiver, radar-type systems cannot be used to measure the path length correction. Because clouds are opaque to visible and infrared radiation, optical sounders will not measure the entire geometric path except for clear sky conditions. We are therefore restricted to passive microwave techniques to evaluate the path length correction.

The microwave spectrum of the earth's atmosphere contains two spectral line complexes of importance for the path length problem. A measure of the distribution of water vapor (and thus e(h)) can be obtained from observations around the 22.235 GHz water vapor line. Similarly, a measure of the temperature and pressure distributions can be obtained by observations around the

2

60 GHz oxygen band. In each case, the quantum physics of the line formation is sufficiently well understood that the uncertainties in the atmospheric parameters dominate the uncertainties in the transition rates over most of the range of conditions of interest to us.

In Figure 1, we give the attenuation spectrum for the whole atmosphere to illustrate the contributions of the various components of the atmosphere. Note that the residual H_2O attenuation is due to the 183.6 GHz water line. Further, over the region of interest to us (1.4 to 10 GHz) the frequency dependence of the absorption is small (in a cloud free case). In Figure 2, we give the brightness temperature spectrum corresponding to Figure 1. Note that the atmosphere is opaque within the 60 GHz oxygen band due to pressure broadening. The 22.235 GHz water vapor line is still partially transparent, however. In order to observe the contributions from the higher altitudes, it is necessary to make use of the line wings particularly for the oxygen band.

The time dependence of the atmospheric index of refraction, and therefore the path length correction, is dominated by the variations in atmospheric water vapor content. The variations in the atmospheric water vapor content can be thought of as corresponding to three levels of spacial structure:

1. Macrostructure: Typical sizes are of the order kilometers. These structures correspond to meteorological phenomena such as "bermuda" highs and large cyclones.

2. Mezzostructure: The characteristic size of these structures is a few hundred meters. These structures correspond to typical clouds and are the principal cause of atmosphere-induced fringe phase fluctuations with short-baseline (1-5 km) interferometer systems.

3. Microstructure: These structures are a few meters or less across and are the cause of non-ionospheric scintillations. It should be pointed out that the division into size regimes is strictly arbitrary. Except for stable cells, a continuum of sizes is almost always present.

Only a relatively limited body of information has appeared on the characteristics of the various size scales. This is particularly true for the microstructure. It is important that additional observations be obtained so that the detailed importance of each effect be determined.

Current remote sensing systems directed toward satellite applications are concerned mostly with the macroscale water vapor structure. Various
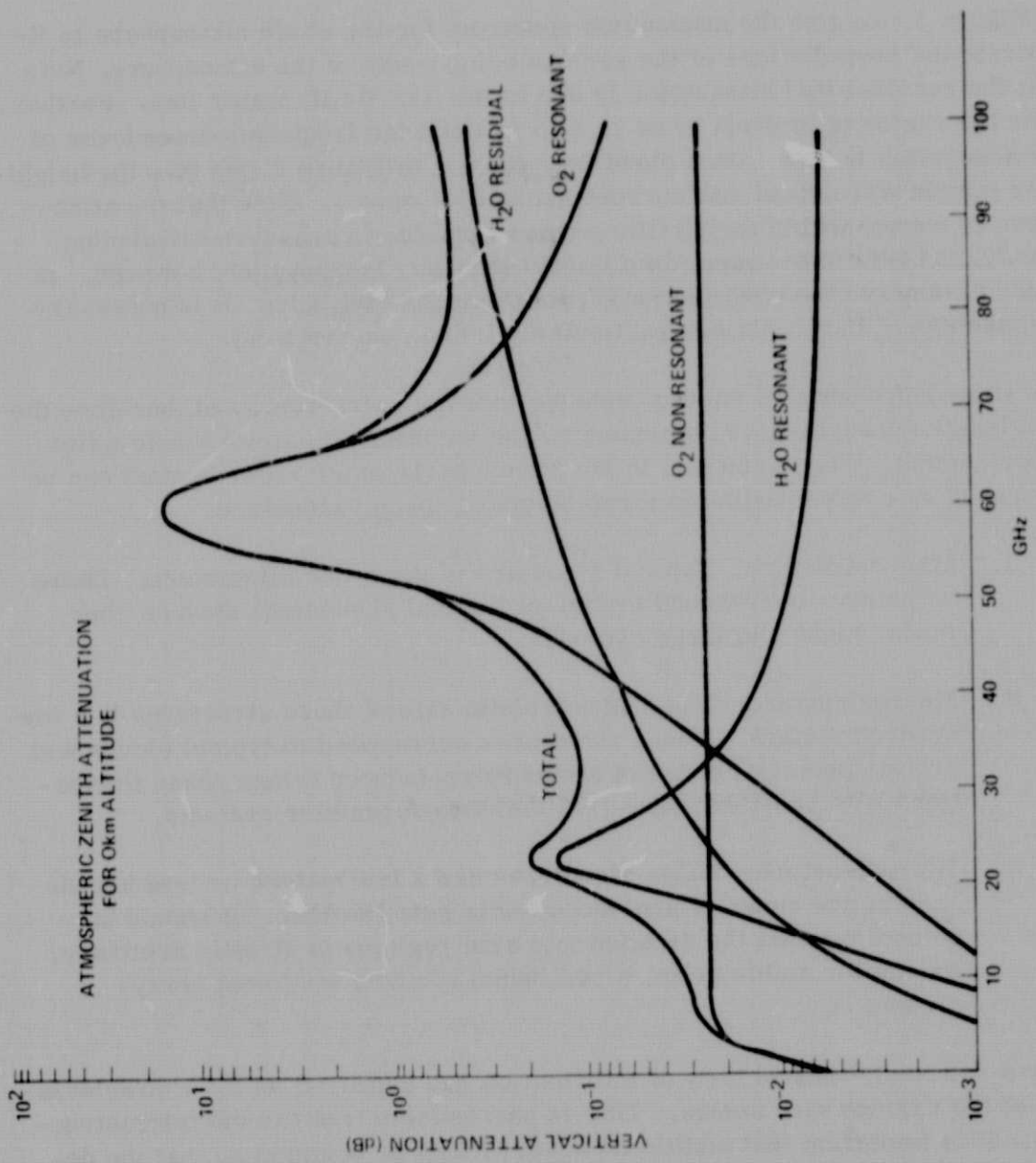
3

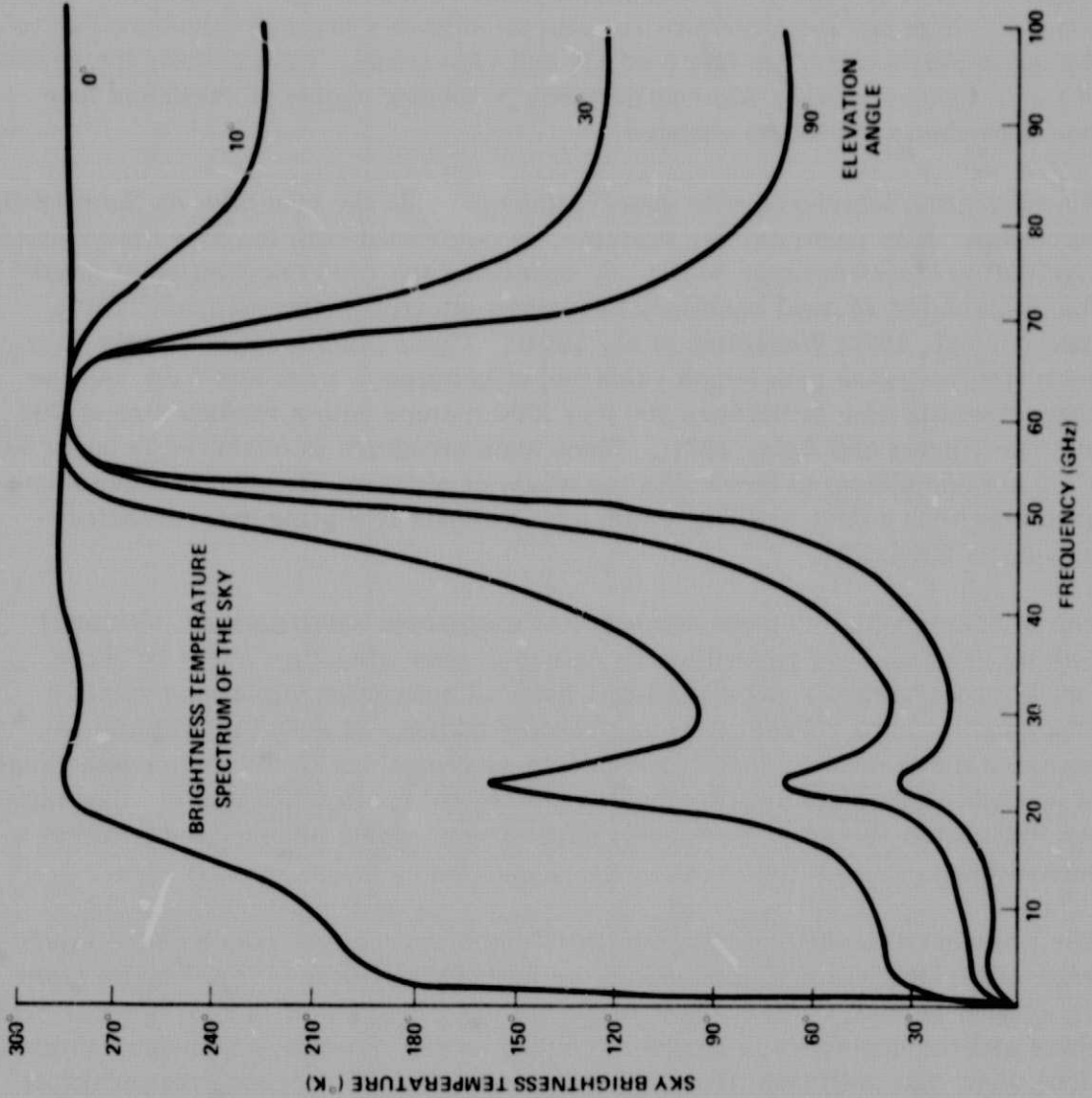Figure 1. Attenuation Spectrum for the Entire Atmosphere under Cloud-Free Conditions

4

Figure 2. Brightness Temperature Spectrum Corresponding to Figure 1

5

experiments (i.e., Rosenkranz et al, 1972; Staelin et al, 1973; Wilheit et al, 1975) show that the variation of precipitable water between two macrostructures, while typically 1/2 to 1-1/2 gm/cm^2, can be as great as 4 gm/cm^2 The time scale for this change depends on the speed of the structure's movement and can be as short as 20 minutes or as long as several hours. Path length changes of nearly 1/2 meter can occur in this period. The fronts which bound the high and low pressure regions often have a layered structure due to the intrusion of warm air into cold air and vice versa. As a result, the region of the boundary between macrostructures is often a region of rapid and location dependent path length changes.

Short baseline interferometer observations provide the best data on the mezzostructure. It is possible, for example, to determine both the size distribution and motion of water vapor "cells" by observing the time correlation of phase fluctuations for several baselines of a given interferometer (Hinder, 1970; Basart et al, 1970; Wesseling et al, 1974). These studies show that the mezzostructure causes path length variation of between 0.1 cm and 5 cm and the characteristic size is between 300 and 1200 meters with a median size of 700 meters (Hinder and Ryle, 1971). Since such structure is observed to occur at 1 - 2 km and seems to move with the winds at altitude, we need to make measurements with a time scale as short as 5 seconds to distinguish the fastest moving of the cells.

The microstructure is responsible for tropospheric scintillations. Virtually nothing has appeared regarding the nature of such structure but it is likely that microstructure represents local index of refraction variations within a cloud and perhaps corresponds to turbulent eddies. It would be difficult to separate the ionosphere and tropospheric scintillations in the wavelength range of interest to us since the two species of irregularities will yield similar angular fluctuation spectra. Frequency dependences would be required to affect a separation.

The procedure for determining the path length correction from passive microwave observations must of necessity be a statistical one. This results from the lack of perfect correlation between the distributions of meteorological variables and the measured brightness temperatures. Radiative transfer calculations show that individual frequencies have an altitude response that peaks at an altitude which depends on the frequency distance from the two major line complexes. An example of these dependences, called weighting functions, is given in Figure 3. Here we plot the normalized weighting function:
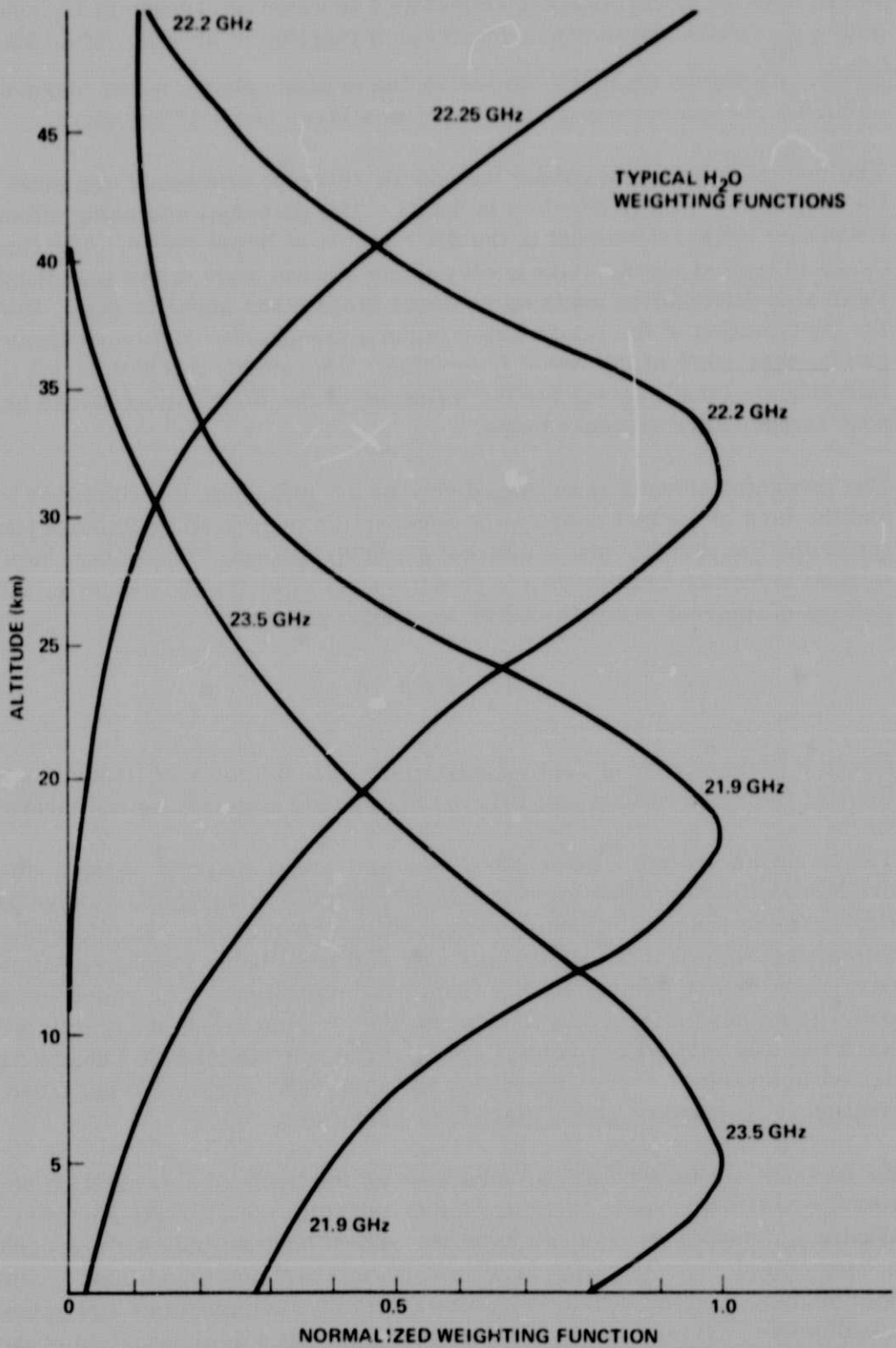
$$W_\nu(h) = \alpha_\nu(h) / \rho_{H_2O}(h) \tag{4}$$

6

Figure 3. Normalized Weighting Functions for Frequencies Around
the 22.235 GHz Water Vapor Line

where α is the absorption coefficient as a function of altitude at frequency ν and ρ_{H_2O} is the water vapor density as a function of altitude (after Staelin, 1966). As can be seen, the emission due to atmospheric water vapor at any particular frequency comes mostly from a layer about 15 km thick.

The inversion procedure must include all relevant processes and must treat the radiative transfer problem in detail. The principal confusing effect in the frequency range of interest is the distribution of liquid water. The liquid drops in typical clouds make a very minor contribution to the path length since their size distribution contains no drops larger than about 50 mm. However, the contribution of the liquid water to the atmospheric brightness temperature can be over 100% of the liquid free value. Therefore, the path length correction scheme must correct for the influence of the liquid water on the brightness temperature measurements.

The inversion scheme is arranged so that the influence of radiometer noise and the lack of perfect correlation between the measured brightness temperatures and the parameters of interest are both treated. The details of the statistical inversion procedure are given in Gaut et al (1972). Briefly, the parameters of interest are obtained by a matrix operation:

$$\overline{P} = \overline{\overline{D}} \cdot \overline{d} \tag{5}$$

where $\overline{p}$ is the vector of derived quantities, $\overline{d}$ is a vector of linear combinations of the observations and $\overline{\overline{D}}$ is the matrix which performs the inversion.

The inversion matrix $\overline{\overline{D}}$ is obtained by a statistical analysis of the computed brightness temperatures for a series of observed atmospheres whose properties span the range of atmospheric conditions of interest. The advantage of this approach is that the parameter vector $\overline{p}$ must be an improvement over a parameter vector derived wholly from local statistics. The result of having noisy brightness temperatures or of having no measurements is to force $\overline{p}$ toward the local statistical value. Modifications of this simple scheme are required to account for non-linearities and to avoid a singular $\overline{\overline{D}}$ but these modifications are based on sound statistical principles.

An analysis of this type can also be used as the basis of a simulation study to find the best instrument configuration and predict the ultimate accuracy obtainable. Schaper et al (1970) have performed such a study for a specific frequency complement (22, 24, 52.65 and 53.65 GHz) and found that, together with surface meteorological variables (humidity, temperature and pressure), a radiometer system with $0.2°K$ accuracy permits a determination of the zenith

path length correction to 1.1 cm. A similar study will be reported in Section III.

II. THE CURRENT STATE OF INSTRUMENT DEVELOPMENT FOR PASSIVE MICROWAVE RADIOMETRY

Instruments employed in passive radiometry will seem insensitive by the standards of present day radio astronomy. In a radiometer, sensitivity is usually less important than absolute stability and accuracy; a useful radiometer for a remote sensing system must have exceedingly great stability and an accuracy (reproducibility) substantially better than most conventional radio astronomy receivers. Thus, an entirely different set of design criteria is required for passive microwave radiometry.

Front end amplifiers, such as parametric amplifiers, cannot be applied to radiometer receivers because their gains cannot be determined with sufficient accuracy and their absolute stability cannot be controlled. The traditional noise tube calibration, even when attenuated to the same level as the incoming signal, is useless because the absolute thermodynamic scale is not repeatable even when the noise tube remains on continuously. Further, it is extremely difficult to determine the attenuation of a precision attenuator to the accuracy required for use with a noise tube calibration.

For these and other reasons, remote sensing radiometers are normally mixer receivers with Dicke switching. Latching ferrite circulators are used for switching and the entire radiometer is normally contained in a temperature controlled enclosure. Both the Dicke load and the enclosure are usually maintained at a temperature slightly above ambient to improve thermal stability even though this may increase the power requirements.

Instrumental calibration usually proceeds in two ways. In the first procedure, the radiometer input (usually a horn antenna at the frequencies of interest to us) is surrounded by an enclosure of Eccosorb or similar microwave black body material of known temperature and the radiometer output is observed. This yields a calibration point at high brightness temperature (perhaps $280^\circ k$). The input is then immersed in a similar enclosure containing boiling liquid nitrogen. This yields a calibration point at low temperature ($77^\circ k$). Temperature coefficients for the various waveguide and switch losses are obtained by observing the high brightness temperature load while the physical temperatures of the components vary. These measurements serve to set the absolute levels of the components independent of measurements of the sky brightness temperature.

9

To handle variations in the effective gain during observations, the temperatures of all the temperature dependent components in front of the Dicke switch are monitored by thermistors. Additionally, a latching circulator is located immediately aft of the antenna so that calibration loads can be switched into the signal path in place of the antenna. In modern receivers, these loads are always thermally compensated resistors. In the many systems, one is at a temperature higher than the highest brightness temperature expected while the other is lower than the lowest expected brightness temperature. Should it prove impossible to obtain a low calibration low enough, it is necessary to depend on a linear receiver characteristic to extrapolate two high calibrations downward.

In the past, satellite instruments have used either a radiation cooled load or else a horn viewing "cold" space to obtain a low reference. Ground based and aircraft instruments have used a boiling liquid nitrogen reference. A precision load and platinum resistance thermometer are immersed in a Dewar containing the boiling liquid nitrogen. Boiling liquid nitrogen has the advantage that the temperature is set by a phase transition whose temperature is very stable as long as atmospheric conditions (pressure) are reasonable. Thus thermal gradients are suppressed. Further, the thermal capacity of liquid nitrogen is not so high as to be a hazard unless one insists on being "aggressively stupid."

Both varieties of reference loads must be carefully temperature controlled so that their emissivity is invariant and their temperatures are well defined. In practice, the best systems allow gradients in the loads of $0.1^{\circ}k$ at most. This has proved to require considerable care but has yielded the advantage that the cold load Dewar need not be filled for nearly 5 hours.

In the rest of this section, we will discuss the characteristics of two instruments which illustrate these design considerations. There are the microwave spectrometer now in operation on Nimbus 5 (NEMS) and the 37 GHz sky temperature radiometer used on the NASA CV 990 during the Bering Sea Experiment.

The Nimbus 5 microwave spectrometer (NEMS) consists of five 250 MHz bandwidth receivers centered at 22.235 GHz, 31.4 GHz, 53.65 GHz, 54.90 GHz and 58.30 GHz. The purpose of the experiment is to sound the temperature, pressure and water content of the atmosphere in nearly all weather conditions (Staelin et al, 1972; Staelin et al, 1973). Each receiver is a load-switched, double-sideband, superheterodyne receiver with a relative accuracy of 0.1 - $0.2^{\circ}k$. In Figure 4, we give a block diagram of a typical NEMS receiver. The two calibration loads are maintained at $215^{\circ}k$ and $296^{\circ}k$ while the Dicke reference load is maintained at ambient temperature. The instrumental time
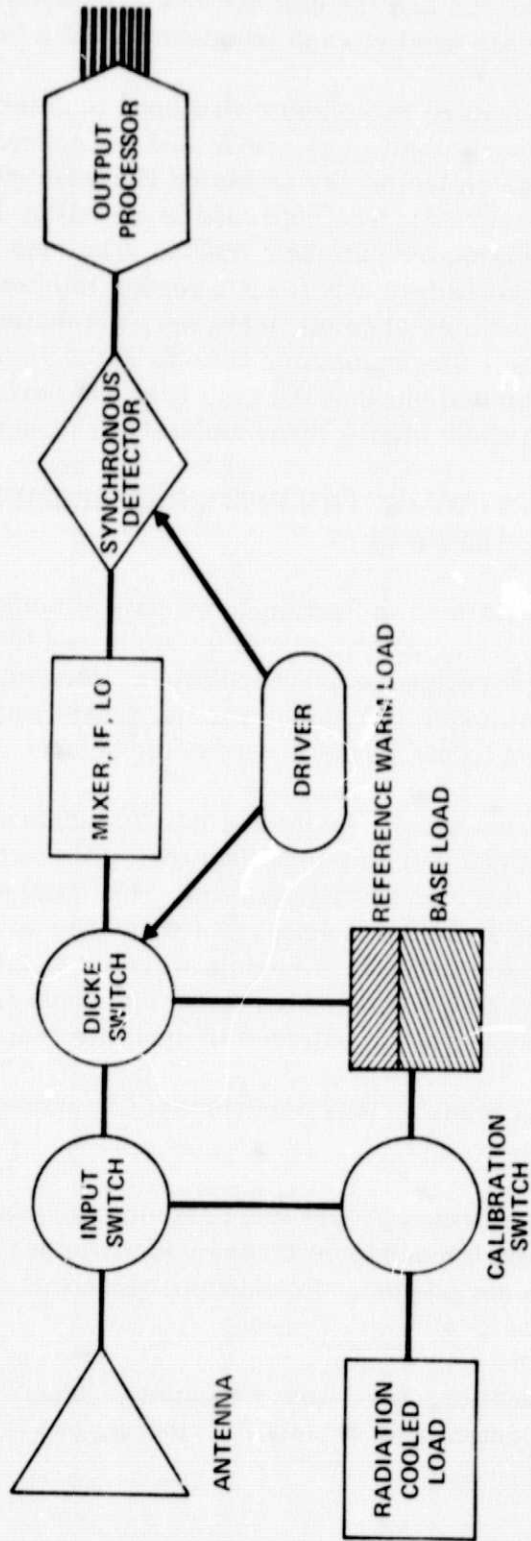
Figure 4. Block Diagram of a typical NEMS Receiver

11

constant is about 2 seconds and the calibrations are observed every 256 seconds. The horn antennas used at each frequency yield a beamwidth of $10°$.

The CV 990 sky temperature radiometer was used to determine the liquid water content of clouds (Wilheit et al, 1975) and for correcting surface emission measurements for reflected sky emission (Webster et al, 1975). A block diagram is given in Figure 5. The cold load is in boiling liquid nitrogen, while the hot load is maintained at about $300°k$. The rms uncertainty in the measured sky temperature is $0.9°k$ for a 1 second integration. Because of the need for the highest possible absolute accuracy, the instrument only views the sky for 1/3 of the time. The remaining time is spent viewing the hot and cold loads. It should be pointed out that the cold load has performed without any difficulty even during short high-g turns and zero-g maneuvers.

III. A SIMULATION STUDY OF THE PPME REQUIREMENTS FOR PATH LENGTH MEASUREMENTS

Using the techniques outlined in Section I, we have simulated the performance of a path length measurement system and so optimized the choice of frequencies for the final sensor package. This study is based on a formulation developed by T. T. Wilheit and T. C. Chang for the Seasat Phase A Study (1973) and the reader is referred to the Phase A report for details.

To summarize, the atmosphere is divided into 100 layers. The sensor package is assumed to include surface temperature, pressure and humidity measurements as well as microwave radiometers. The microwave sky temperatures were calculated from the best current transition probabilities and line formation theory. The atmosphere models were taken from the Handbook of Geophysics and Space Environments and span the range from arctic to tropical conditions. Cloud models were selected to span the range of most cloud types.

Before reviewing the results, it is appropriate to summarize the implicit and explicit assumptions:

1. The Handbook atmospheres are assumed to span the conditions of interest. Thus temperature inversions and other deviations from the models are not treated. In addition, temporal variations were not treated.

2. Cloud attenuations have been assumed to depend only on the total liquid water content and Rayleigh scattering has been assumed.
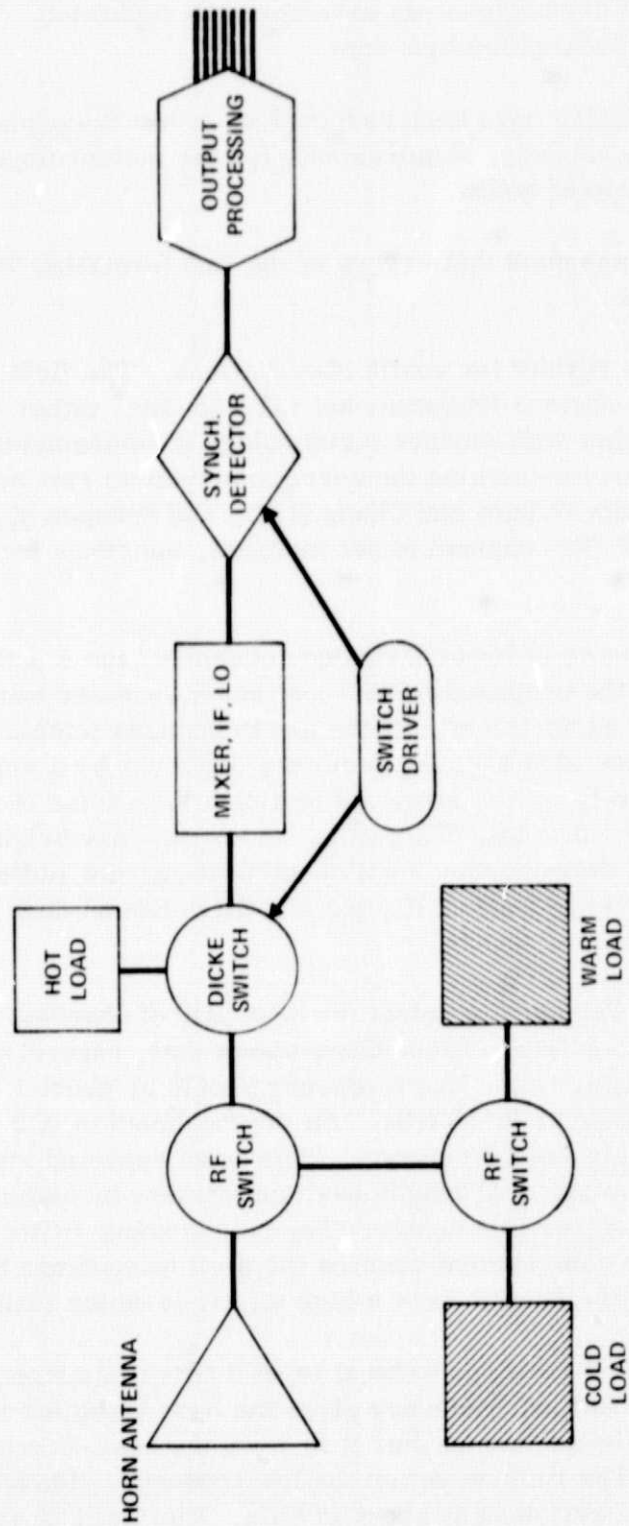
12

Figure 5. Block Diagram of the CV 990 Sky Temperature Radiometer

13

3. The wet and dry components have not been separated. The integral has been approximated by a sum.

4. The radiometers have been assigned an rms measurement noise of $0.5°k$. The accuracy requirements for the meteorological sensors will be discussed below.

5. It has been assumed that errors in the line formation theory make no contribution.

We first examine the results for zenith observations. The first major conclusion is that the most obvious frequency set (22.235 GHz, either 18 or 31.4 GHz and 53.29 GHz) together with surface meteorology measurements (humidity, pressure, temperature) determine the correction with an rms accuracy of 1.8 cm. In agreement with Wilheit and Chang (1973) and Schaper et al (1970), we find that, if the 53.29 GHz channel is not included, the error increases to 2.2 cm.

As a test of the necessity of lower frequency channels, the 8.4 GHz off-source measurements from the proposed PPME continuum receiver were included with the 18, 22.235, 53.29 triplet. If the sky brightness temperature is measured with an rms noise of $0.1°k$, the accuracy improves by a small amount (0.1 cm). Alternatively, if the more conventional rms noise of $0.5°k$ occurs, the error increases by 0.2 cm. Therefore, unless the sky brightness temperature is measured to the accuracy level of the best current radiometers (i.e., the NEMS experiment; see Section II), the 8.4 GHz channel does not significantly improve the determination.

An iterative scheme was used to select the best pair of channels near the 22.235 GHz water vapor line. The scheme shows that, regardless of the second frequency, the water vapor line frequency should be about 1 GHz from the line center, i.e., either 21 or 23 GHz. An improvement of 0.2 - 0.3 cm results depending on the second frequency. This is as expected since the percentage contribution to the total brightness temperature by higher altitude water vapor is greater off the line center. The region about 1 GHz from the line center is an effective compromise between the need to measure the high altitude water vapor and the need to have a high signal-to-noise ratio.

The second frequency is required to be at least 2 GHz away from the near-line frequency. Since the second frequency gives the correction for the presence of liquid water, within limits, the farther it is from the near-line channel, the lower the error is. The limit is set on the low frequency side by the need for a high signal-to-noise ratio and is about 17 GHz. The limit is set on the high

14

frequency side by the increasing contribution from the oxygen band at 60 GHz, and is about 40 GHz.

In Table 1, we give the rms error in the path length determinations and the total correlation between the measurements and the path length for a selection of the frequency pairs which show the lowest errors. Note that the 18 and 19 GHz pairs are essentially identical. An extension to 31 GHz results in a slight improvement. Because of the sharpness of the local minimum in the sky brightness temperature between the water vapor line and the oxygen, moving 1 GHz or more away from 31 GHz notably degrades the performance.

Table 1

Accuracy of Path Length Determination and Correlation of Measurements

Frequency Pair		RMS Error	Correlation
(GHz)		(Cm)	(%)
18	21	2.23	97.5
19	21	2.19	97.6
25	21	2.20	97.5
18	23	2.20	97.6
19	23	2.19	97.6
25	23	2.20	97.6
31	21	2.19	97.6
31	23	2.19	97.6

The above calculations have assumed that along with the microwave measurements, the surface humidity is measured to 5%, the surface pressure to 1 mb and the surface air temperature to 2°K. Since the cost of surface meteorological instruments is a very strong function of the desired measurement accuracy, the contribution of improved accuracy for the meteorological instruments must be determined. To illustrate the change in performance for improved accuracy in the instruments, we give in Table 2 accuracies and correlations for the 18 GHz - 21 GHz pair as the accuracy of the meteorology instruments improves. Table 2 shows that the ultimate accuracy contribution of the meteorology instruments increases much more slowly with instrumental accuracy

Table 2

Influence of Surface Meteorology Instruments on Accuracy

Assumed Meteorology Error	Path Length Error	Correlation	Percent Improvement
Humidity 5% Air Temperature 1°K Pressure 2mb	2.23 cm	97.4%	--
Humidity 3% Air Temperature 1°K Pressure 1mb	2.04 cm	97.4%	8%
Humidity 2% Air Temperature 1°K Pressure 0.5mb	2.0 cm	97.4%	10%
Humidity 2% Air Temperature .01°K Pressure .01mb	1.98 cm	97.4%	11%

than the cost. For example, according to T. A. Clark (personal communication), the cost of the last set of instruments is a factor of nearly ten higher than the cost of the third set. Accordingly it is not cost-effective to obtain the accuracy level of the last set in the table. It is however desirable to obtain the accuracy level of the third set since this yields an improvement of 10% for an estimated cost increment of about a factor of 2 (T. A. Clark, personal communication).

We next address the off-zenith problem. The calculations show that the path length varies with the secant of the zenith angle to high accuracy. This is as expected since the path length is the equivalent of the optical air mass which also varies as the secant of the zenith angle. The inversion study shows that the error also scales roughly as the secant. In Table 3 we give the errors and correlations for some of the frequency pairs of Table 1 for zenith angles of 45° and 60°.

Clearly, by 60° zenith angle, the error has reached an unacceptably high level. The PPME goal calls for an accuracy of no worse than 4 cm total at large

16

Table 3

Behavior of the Frequency Pairs for Off-Zenith Observations

Frequency Pair	$z = 45°$		$z = 60°$	
(GHz)	Error (Cm)	Correlation (%)	Error (Cm)	Correlation (%)
18-21	4.22	95.2	6.00	95.1
19-21	4.24	95.1	6.11	94.9
25-21	4.39	94.8	6.21	94.8
18-23	4.28	95.0	6.24	94.7
19-23	4.34	94.9	6.43	94.4
25-23	4.46	94.6	6.50	94.2
31-21	4.21	95.1	5.99	95.1
31-23	4.14	95.3	6.28	94.6

zenith angles. The question arises as to how much of the error is due to the wide span of atmospheric conditions included in the analysis. In the preceding analysis, the total range of atmosphere models covers conditions from clear polar winter to humid cloudy tropic summer. We now restrict the range of atmosphere models to mid-latitude conditions. For each case in Table 1 and 3, the errors are cut by a factor of 2. To illustrate the improvement, we have calculated the 19 and 21 GHz brightness temperatures and path length for the U.S. standard atmosphere and performed the inversion. Since the U.S. standard atmosphere represents the average U.S. conditions, we expect that the inversion will recover the calculated path length to high accuracy. As Table 4 shows, this is the case even for heavy clouds. Therefore, it may be necessary to develop the regression constants for each of the PPME sites from measured atmospheric conditions which span the total range of conditions at the site.

Analyses were also made for three frequency schemes to indicate the influence of the increased path length as the zenith angle rises. The two lower frequencies were fixed at 18 GHz and 21 GHz while the third frequency ranged from 37 to 60 GHz. The region from about 55 GHz to 60 GHz made no contribution to the inversion since the atmosphere is opaque within the oxygen band. In the region from 37 to 50 GHz, the contribution is of the same order as at 31 GHz and becomes progressively worse as the frequency rises. In the region between

Table 4

Inversion of U.S. Standard Atmosphere

19 GHz, 21 GHz, Surface Pressure, Humidity, Air Temperature	
$z = 0°$ 0.1 cm No Clouds	0.1 cm Heavy Clouds
$z = 45°$ 0.6 cm No Clouds	0.7 cm Heavy Clouds

50 and 55 GHz, the brightness temperature is proportional to the temperature and pressure distributions. Therefore, the error decreases somewhat for a third frequency in this range. As the zenith angle increases, the correlation of the third frequency decreases. This is due to the atmosphere becoming optically thick at the larger zenith angles between 50 and 55 GHz. To illustrate this, we give in Table 5 the errors including correlations for the 18 GHz, 21 GHz, and 53 GHz triplet for zenith, 45° and 60° zenith angle.

Table 5

Error and Individual Correlations for the 18 GHz, 21 GHz and 53 GHz Triplet

Zenith Angle (Degrees)	Error (Cm)	Correlations (%)		
		18 GHz	21 GHz	53 GHz
0°	1.8 Cm	84%	57%	83%
45°	3.7	84%	57%	50%
60°	5.8	84%	57%	20%

Thus, a system which will measure the path length correction to the required accuracy should be configured as follows:

1. At least two microwave radiometers (18 GHz, 21 GHz) with 0.5°K rms noise and 1°K long term stability. If a third frequency can be accommodated it should be about 53 GHz.

2. Surface meteorology instruments which measure relative humidity to 3°, air temperature 1°K and pressure to 1.0 mb.

18

ACKNOWLEDGMENTS

BIBLIOGRAPHY

Basart, J. P., Miley, G. K., and Clark, B. G. (1970), Phase Measurements
with an Interferometer Baseline of 11.3 km, *IEEE Trans. Ant. and Prop.*,
AD-19, 375.

Bean, B. R. and Dutton, E. J. (1966), *Radio Meteorology*, NBS Monograph 92,
(Washington: GPO).

Gant, N. E., Reifenstein, E. C., III, and Chang, D. T. (1972), *Microwave
Properties of the Atmosphere, Clouds and the Oceans*, Final Report Con-
tract NAS 5-21624.

Goad, C. C. (1974), *Wallops Island Tropospheric Refraction Study and
Analysis*, Final Report Contract NAS 6-2173.

Hinder, R. A. (1970), Observations of Atmospheric Turbulence with a Radio
Telescope at 5 GHz, *Nature*, 225, 614.

Hinder, R. A., and Ryle, M. (1971), Atmospheric Limitations to the Angular
Resolution of Aperture Synthesis Radio Telescopes, *Mon. Not. Roy.
Astron. Soc.*, 154, 229.

Hopfield, H. S. (1971), Tropospheric Effect on Electromagnetically Measured
Range: Prediction from Surface Weather Data, *Radio Science*, 6, 357.

Marini, J. W., and Murry, C. W., Jr. (1973), *Correction of Laser Range
Tracking Data for Atmospheric Refraction at Elevations Above 10 Degrees*,
X-591-73-351, (Greenbelt: GSFC).

Rosenkranz, D. W., Barath, F. T., Blinn, J. C., III, Johnston, E. J., Lenoir,
W. B., Staelin, D. H., and Waters, J. W. (1972), Microwave Radiometric
Measurements of Atmospheric Temperature and Water from an Aircraft,
Journ. Geophys. Res., 77, 5833.

Schaper, L. W., Jr., Staelin, D. H., and Waters, J. W. (1970), The Estima-
tion of Tropospheric Electrical Path Length by Microwave Radiometry,
Proc. IEEE, 50, 272.

Staelin, D. H. (1966), Measurements and Interpretation of the Microwave Spec-
trum of the Terrestrial Atmosphere Near 1-Centimeter Wavelength, *Journ.
Geophys. Res.*, 71, 2875.

Staelin, D. H., Barath, F. T., Blinn, J. C., III, and Johnston, E. J. (1972), The Nimbus E Microwave Spectrometer (NEMS) Experiment, in Sabatini ed., The Nimbus 5 Users Guide, (Greenbelt: GSFC).

Staelin, D. H., Barrett, A. H., Waters, J. W., Barath, F. T., Johnston, E. J., Rosenkranz, P. W., Gaut, N. E., and Lenoir, W. B. (1973), Microwave Spectrometer on the Nimbus 5 Satellite: Meteorological and Geophysical Data, Science, 182, 1339.

Webster, W. J., Jr., Wilheit, T. T., Ross, D. B. and Gloersen, P. (1975), Analysis of the Convair-990 Passive Microwave Observations of the Sea States During the Bering Sea Experiment, in Kondrat'yev and Nordberg eds., Proc. Symp. Bering Sea Exp. (Leningrad: VMGO) in press.

Wesseling, K. H., Basart, J. P., and Nance, J. L. (1974), Simultaneous Interferometer Phase and Water Vapor Measurements, Radio Science, 9, 349.

Wilheit, T. T., and Chang, T. C. (1973), Microwave Radiometry, in Scull ed., Seasat-A Phase As Study Report (Greenbelt: GSFC).

Wilheit, T. T., Fowler, M. G., Stamback, G., and Gloersen, P. (1975), Microwave Radiometric Determination of Atmospheric Parameters During the Bering Sea Experiment, in Kondrat'yev and Nordberg eds., Proc. Symp. Bering Sea Exp., (Leningrad: VMGO), in press.